

## THE CLUSTERS NGC 419 AND NGC 416 IN THE WING OF THE SMALL MAGELLANIC CLOUD

DANIEL DURAND AND EDUARDO HARDY<sup>1</sup>

Département de Physique and Observatoire du Mont Mégantic, Université Laval, Québec

AND

JORGE MELNICK

Astronomy Department, University of Chile

Received 1983 December 27; accepted 1984 February 24

### ABSTRACT

We have constructed deep color-magnitude diagrams, based on du Pont plates, for the rich clusters NGC 419 and NGC 416 located in the Wing of the Small Magellanic Cloud. Use of radial star counts in the clusters and a statistical decontamination technique, which employs the information of the surrounding field, have allowed us to isolate the stellar populations of the clusters from that of the dense background in which they are immersed. Integrated photometry in the Washington system provides a lower limit to their metallicity of  $[Fe/H] = -1.0$ . Fits of the evolved main sequences to the Yale isochrones, which are dependent on the uncertain distance and reddening scales, indicate ages of  $1.2 \pm 0.5$  Gyr for NGC 419 and  $2.5 \pm 0.7$  Gyr for NGC 416. The quoted errors are believed to be representative of the combined uncertainties. The presence of an age difference is consistent with published statistics on the number of bright red giants and carbon stars. The  $\sim 1.5$  Gyr value of the age difference, which is essentially independent of the distance scale, is consistent with published photometric classification indices.

*Subject headings:* clusters: open — galaxies: Magellanic Clouds — galaxies: stellar content — stars: evolution

### I. INTRODUCTION

The clusters NGC 419 and NGC 416, shown in Figure 1, are two of the brightest and richest members of the Small Magellanic Cloud (SMC). They dominate the "Wing" region of the SMC, a region characterized by its distorted shape and by a large density of field stars, and which corresponds to the SMC eastern extension toward the Large Magellanic Cloud (LMC).

No firm values for the ages of these two clusters exist. Arp (1958*b*) constructed the first color-magnitude diagram (CMD) for NGC 419 but only to relatively bright magnitudes, while Walker (1972) obtained deeper (electronographic) exposures but over a somewhat restricted area. As a result, the published CMDs were either limited in magnitude or in the statistics of cluster members and did not provide a clear description of the sequences. No diagram for NGC 416, on the other hand, has ever been constructed except for a preliminary and uncorrected version of a subsample of the same data presented here (Hardy, Melnick, and Rhéault 1980), which also included a preliminary diagram for NGC 419.

In this investigation we construct CMDs for both clusters in an effort to place them in the age-metallicity plane for the Magellanic Clouds (Hodge 1983, and references therein). In this we join a number of workers trying to unveil the peculiarities of star formation and chemical evolution in environments different from that of the Galaxy. The Magellanic Clouds offer the unique possibility of allowing direct calibrations of clusters for which ages and metallicities are related in a special way. An associated study of the *field* of the SMC Wing, directed toward the analysis of the superposition of epochs of star formation has already been published (Hardy and Durand 1984, hereafter Paper I).

### II. OBSERVATIONS AND DATA REDUCTION

The plate material as well as the procedure followed to obtain final magnitudes is the same described in Paper I. Four visual limiting exposures (103a-D + W16) and four limiting blue exposures (103a-O + W2C) were obtained with the 2.5 m du Pont telescope at Las Campanas (scale =  $10^{\circ}9$  mm<sup>-1</sup>; field =  $1^{\circ}5 \times 1^{\circ}5$ ) under good seeing conditions (FWHM = 1"). The areas shown in Figure 1 were digitized in Geneva with the ESO Optronics microdensitometer using steps of  $0.33 \mu\text{m pixel}^{-1}$ . The fully automatized reduction procedure (Durand 1982) takes into consideration: (1) the presence of crowding, (2) the need to obtain accurate magnitudes inside a dynamical range of almost 5 mag, (3) the use not only of the standard stars but of all stars in common between plates to perform the final reduction into standard magnitudes (Stetson and Harris 1977), and (4) the need to isolate the annular section of the clusters for which the contrast against the background is optimized.

We proceeded as follows. The data were transformed into intensity units via calibration-wedge images exposed onto the plates shortly after the stellar exposures. The calibration sequence, used for both clusters, was derived from the list of electronographic *B* and *V* magnitudes of Walker (1972) in NGC 419. To this end, an image of the area containing NGC 419 was displayed on an image monitor, and the digital intensity contrast was manipulated so as to unmask the degree of stellar contamination of each stellar image. Once the selection of standards was completed, an automatized algorithm was tested which rejected the contaminated images on the basis of the presence of multiple centers. The same rejection criterion was used later in the "batch" treatment of all the data. A total of 59 stars out of the 146 measured by Walker (1972) and Arp (1958*b*) were retained as standards. As described in Paper I, these stars provided the zero point and the magnitude scale of the photometry.

<sup>1</sup> Guest Investigator, Las Campanas Observatory of the Carnegie Institution of Washington.

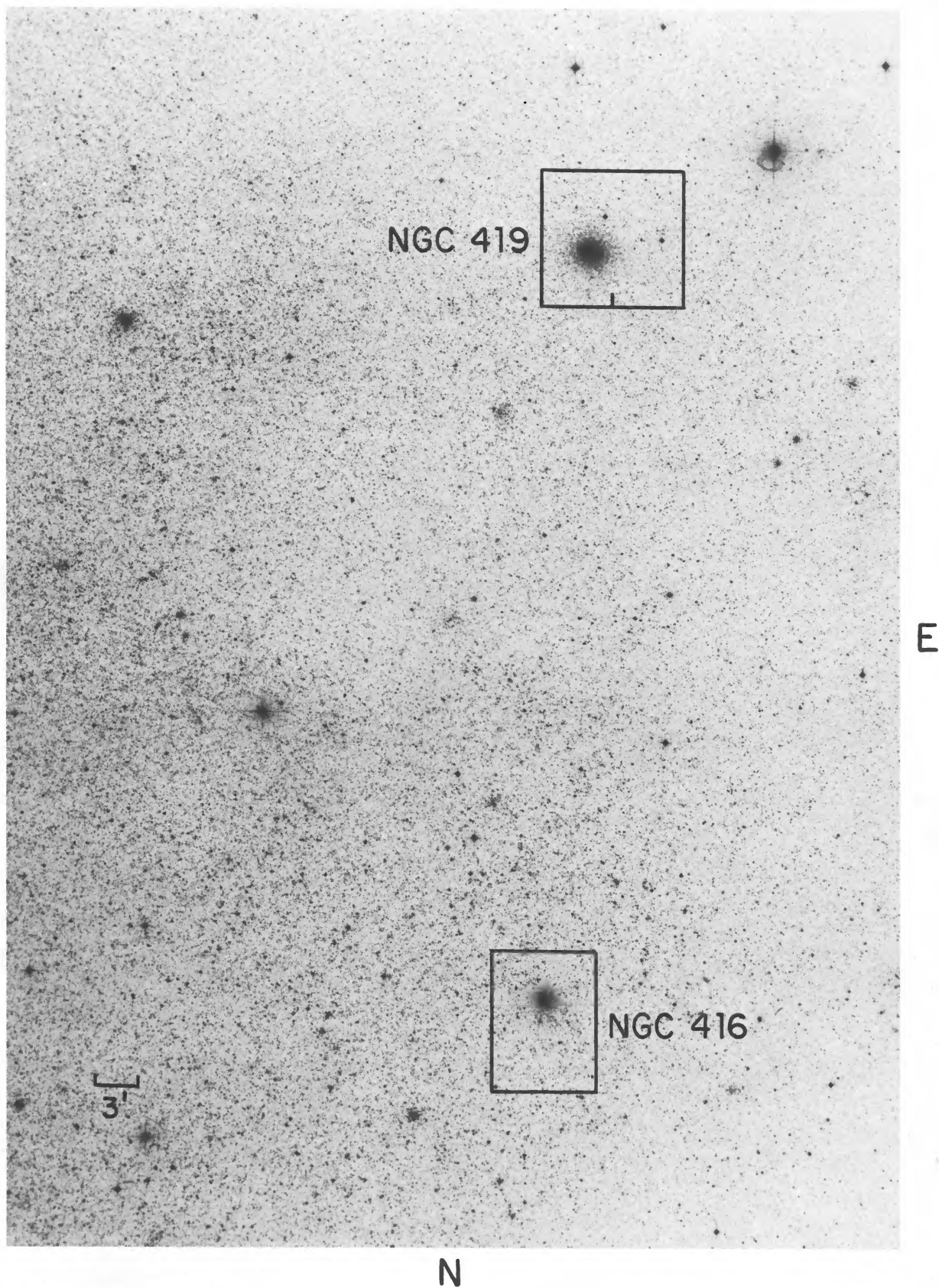


FIG. 1.—A blue limiting exposure with the du Pont 2.5 m telescope of the cluster regions studied in the SMC Wing. The side of the square enclosing NGC 419 corresponds to 6'. The tick mark in NGC 419 corresponds to the position of  $R_2$  in Fig. 2.

Stellar images were identified and accepted, or rejected, automatically. Instrumental magnitudes were obtained through a variation of the  $\Sigma$ -method of pixel summation of Newell and O'Neil (Rhéault and Hardy 1980) implemented with a circular aperture and with the background determined from an external annulus. After background subtraction, each pixel was weighted by its information content (i.e., its intensity) in what amounted to adding the squares of the intensities before passing to logarithmic scale. This procedure has been shown, in practice, to provide a significant increase in internal precision while reducing, at the same time, the contribution of faint contamination pixels. The price to be paid is, of course, the destruction of the linearity of the final calibrating relationship, a consideration of little importance in our case since no extrapolation of the instrumental versus standard magnitude diagram was required. A further modification to the original  $\Sigma$ -method was introduced. Because the precision of the magnitude determination as function of magnitude depends critically on the size of the numerical "diaphragm," a continuously variable aperture function was established for each plate using the standard stars as a guide. No *single* numerical integration aperture was able to reproduce the internal accuracy of the variable aperture method for both bright and faint stars. The same aperture function was used for standard and program stars, this being the fundamental constraint of the method.

Finally, the procedure outlined by Stetson and Harris (1977) was used to merge numerically all plates in each bandpass on a common instrumental system. Briefly, each star on each of the plates of a given bandpass was transformed to the instrumental-magnitude system of the "base" plate using Chebyshev interpolation. The average of four plates, for each bandpass, provided a more precisely determined instrumental system before reduction into standard magnitudes and used the information contained in all stars in common—and not only the standard stars—to generate the final magnitudes in the Johnson  $BV$  system. A small color correction, found as part of the procedure, was applied to the data. Inspection of the calibration curves of Figure 3, 4, and 5 of Paper I shows that this procedure succeeded in reducing the scatter of the fainter half of the standards to  $\sigma_{B,V} < 0.1$  mag.

### III. BACKGROUND SUBTRACTION AND THE CLUSTER DIAGRAMS

Inspection of Figure 1 should suffice to convince the reader that unless extreme care is taken to isolate the clusters from the dense stellar background in which they are immersed, one is likely to derive the properties of the field rather than those of the clusters. To avoid such an occurrence we followed a twofold procedure. First, we used the stellar-identification algorithm to derive stellar densities and isolate the annular regions, centered on the clusters, for which the contrast with the superposed background was a maximum. Second, once the CMDs for the annuli were obtained, a procedure was applied to eliminate the background "noise" in a statistically sound way using the CMD of the surrounding field.

Figure 2 displays the stellar surface density curves for the two clusters expressed in units of number of stars (counted in the  $V$  bandpass) per 100 arcsec<sup>2</sup>, as function of radial distance  $R$  in arcsec. Because of the unknown degree of completeness we are not attempting here to fit models (i.e., King 1966) to the density profiles. One should notice, in particular, the non-monotonic behavior of the curves near the cluster centers, due to rejection of crowded images. This explains why the regions of maximum contrast with respect to the field cannot include

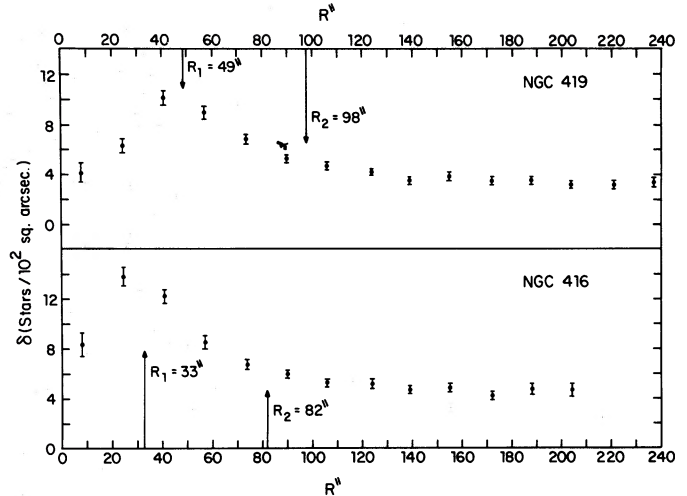


FIG. 2.—Density of stars as function of radial distance from the cluster centers. The radii defining the annuli used for the construction of the CMDs are indicated. Notice the sudden drop in density near the center of the clusters due to the rejection of contaminated images.

the cluster centers. The internal and external radii  $R_1$ ,  $R_2$  of the cluster annuli determined from visual inspection of the curves are indicated, and they define the regions to be preferred for the construction of the cluster "total" (i.e., contaminated) diagrams. The "field" diagrams are then constructed farther out than  $R_2$  outside an assumed tidal radius of  $2'$  (i.e.,  $\sim 30$  pc). The field diagram for NGC 419 is presented in Figure 3 together with a number of observational sequences which are described in the legend and which provide a check on our magnitude and color scales. A detailed discussion of this CMD is given in Paper I, where it is shown that the field diagrams thus constructed are identical with those of an *isolated* field area.

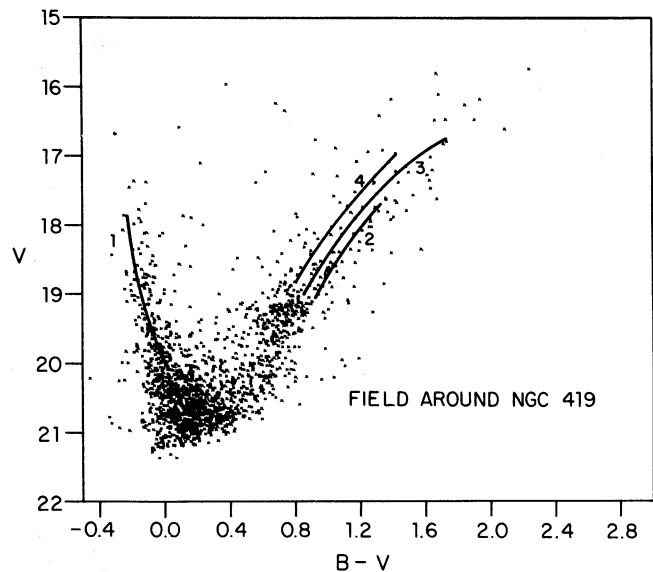


FIG. 3.—The CMD for the field around NGC 419 (i.e., external to a radius of  $98''$ ). The schematic numbered sequences represent: (1) the main sequences for NGC 419 and NGC 458 (Arp 1958b), (2) the field red-giant branch for the W side of the SMC (Brück and Hawkins 1981), (3) Arp's (1958a) giant branch for the field near NGC 419, and (4) the field red-giant branch for the NE outer regions (Brück and Marsoglu 1978).

To obtain the decontaminated CMDs from the subtraction of both diagrams we have proceeded as follows. First, the total and field CMDs for each cluster were binned in  $V$  and  $B-V$ . Then the field CMD was normalized to the area of the total diagram, rounding off the resulting bin population to the nearest integer value, and the resulting CMD was subtracted bin-per-bin from the total diagram. In order to keep the "structure" of the original CMD as unchanged as possible, the bin-per-bin subtraction was carried out as follows: if  $m$  stars were identified in the field CMD and  $n$  stars in the total diagram (with  $m < n$ ), then  $m$  stars were "erased" randomly from the corresponding bin in the total CMD, the remaining stars conserving their position inside the bin. If, on the other hand,  $m > n$ , the resulting bin population was set to zero.

Experiments were performed to decide on the best bin size so as to reduce the occurrence of " $m > n$ " situations, due to statistical fluctuations in very small bins, or the excessive deformation of the SMD due to very big bins. We finally settled on square bins of size 0.1 mag. The procedure outlined here resembles that which had been applied by Hodge (1981) to NGC 152, on the opposite side of the SMC.

#### IV. ANALYSIS OF THE COLOR-MAGNITUDE DIAGRAMS

##### a) Global Features

Figures 4a and 5a show, respectively, the CMDs for NGC 419 and NGC 416 inside the annuli of Figure 2, prior to the decontamination procedure. Stars brighter than  $V = 16$  have

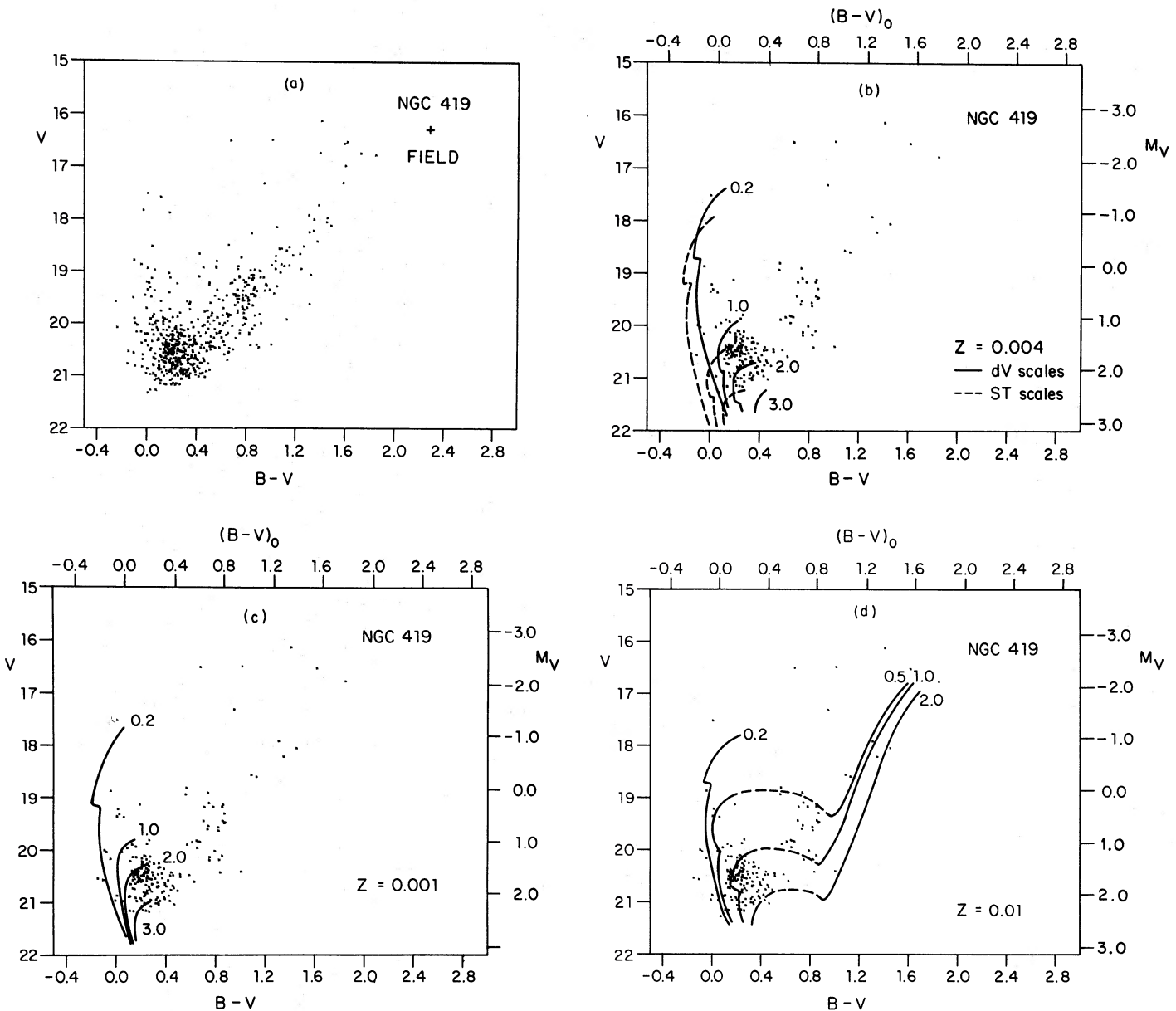


FIG. 4.—(a) The CMD for NGC 419 inside the annulus of Fig. 2 with the contribution of the background population unremoved. Notice the presence of a subgiant branch linking the main sequence to the "clump." (b) The decontaminated diagram for NGC 419 with the Yale isochrones for  $Z = 0.004$  and for the dV and ST scales superposed. The absolute axes have been labeled on the dV scale. Ages are in Gyr. The Hertzprung gap is now apparent. (c) Same as Fig. 4b but for  $Z = 0.001$  and the dV scale. (d) Same as Fig. 4c but for  $Z = 0.01$ .

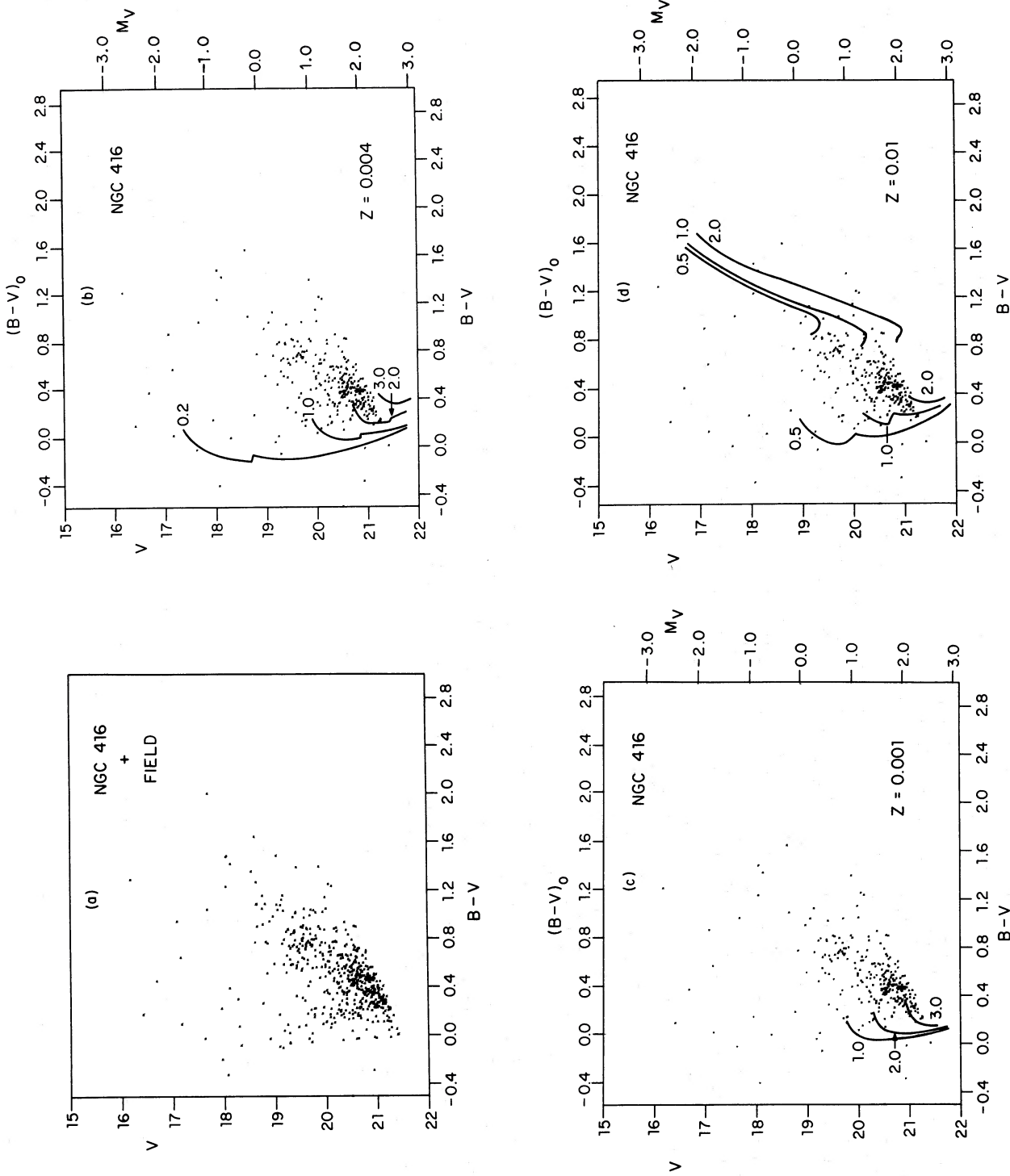


FIG. 5.—(a) The CMD for NGC 416 inside the annulus of Fig. 2 with the contribution of the background population unremoved. (b) The decontaminated diagram for NGC 416 with the Yale isochrones for the  $dV$  scale and  $Z = 0.004$ . The absolute axes have been labeled on the  $dV$  scale. (c) Same as Fig. 5b for  $Z = 0.001$ . (d) Same as Fig. 5c for  $Z = 0.01$ .

TABLE 1  
INTEGRATED PHOTOMETRY IN THE WASHINGTON SYSTEM

Cluster	$C-M$	$M-T1$	$T1-T2$	$n$	$Q_{CMT1}$	[Fe/H]
NGC 419.....	$0.614 \pm 0.004$	$0.637 \pm 0.005$	$0.545 \pm 0.015$	2	0.450	$\geq -1.0$
NGC 416.....	$0.657 \pm 0.007$	$0.663 \pm 0.014$	$0.526 \pm 0.014$	2	0.461	$\geq -1.0$

been excluded because of image saturation. The core-helium-burning “clump,” which represents the horizontal branch of Population I (Flower 1984) discussed in Paper I, is present in all diagrams.

In the case of NGC 419 there is a clear indication of a discontinuity in the density of stars along the main sequence near  $V = 20$ , indicating that a turnoff for the cluster has been reached (compare with Fig. 3). For NGC 416 the situation is less clear because of the smallness of the sample. After decontamination, the turnoff of NGC 419 (Fig. 4*b*) is well established, as is the presence of a Hertzsprung gap. The populated subgiant branch present in the field (see Fig. 3), which is discussed in Paper I as providing evidence that the field contains a population at least as old as 3 Gyr, has disappeared. In the case of NGC 416 (Fig. 5*b*) the main-sequence discontinuity is now more clearly displayed and is located about 0.5 mag fainter and 0.2 mag redder than in NGC 419. Notice that the main difference between the diagrams of Figures 5*a* and 5*b* arise in the subgiant branches and, particularly, in the bright blue main sequence clearly decimated by the decontamination procedure.

How reliable are, from a statistical standpoint, the decontaminated diagrams? The same procedure leading to the bin-per-bin subtraction can be used to estimate the statistical weight of each bin in the subtracted diagrams by evaluating the Poisson errors associated with the numerical differences between corresponding bins. Call  $N_T$  and  $N_F$  the “total” and “field” population of each bin; the true bin population of the cluster is then  $N_c = N_T - N_F$ , and the associated Poisson error is  $\sigma_c = (N_T + N_F)^{1/2}$ . We have found for the turnoff magnitude levels already indicated that  $\sigma_c/N_c < 0.3$  for both clusters, a result which lends confidence to the reality of the observed discontinuities. Most importantly, the structure in NGC 416 at  $V \sim 20.5$ ,  $B - V \sim 0.5$  in Figure 5*b* appears real and not an artifact of the subtraction process. Notice that our data *have not* been corrected for the magnitude and position-dependent effects of crowding. Because crowding, which affects the faint stars more, is stronger in the dense core of the clusters than in their periphery, where the field diagrams were computed, the effect of the diagram subtraction on the final CMD is to underestimate the resulting faint population. This effect is readily observable in Figure 4*b*, where the density of stars in the main sequence clearly diminishes for magnitudes fainter than  $V \sim 20.5$ . It also reinforces the belief that the main-sequence structure in Figure 5*b* is real while making, on the other hand, the level of its upper termination point more uncertain.

*b) A Photometric Estimate of the Cluster Metallicities*

Prior to any attempted determination of the age of the clusters via model fitting, we must set limits to the assumed abundances. To that end we have used a procedure introduced by Harris and Canterna (1977) which uses the *integrated* colors of the clusters in the Washington system (Canterna 1976). The observations (through apertures of 2') were performed at the du Pont telescope as part of a photometric program partially reported earlier (Hardy 1981), to which we refer the reader for the details of the observational procedure. The results are listed in Table 1, where the columns are self-explanatory. Harris and Canterna (1977) have shown that for *globular clusters* a tight correlation exists between [Fe/H] and the integrated reddening-free parameter,

$$Q_{CMT1} = (C - M) - 1.2[(M - T1) - 0.5],$$

which is superior to the corresponding correlation of the *UBV* photometry. Since NGC 419 and NGC 416 have bright main sequences, their integrated colors (as shown, among others, by Gordon and Kron 1983) are bluer than those of “bona fide” globular clusters of the same metallicity. This effect will simulate a lower metallicity in Figure 4 of Harris and Canterna, and all we can conclude from our Table 1 is that for both clusters the metallicity must be higher than [Fe/H] = -1.0. This lower limit is consistent with other determinations of SMC metallicities for intermediate-age objects; Gascoigne, Bessel, and Norris (1981) give, for example, [Fe/H] = -0.8 for K3 from observations of individual stars.

*c) Ages and the Distance-Reddening Problem*

Because we have no means of attempting a fundamental determination of the distance and reddening we are forced to choose among known scales on the basis of consistency between evolutionary models and the observed evolved main sequence. A number of distance and reddening scales have been proposed for the SMC, and they are listed in Table 2, which supersedes Table 2 of Paper I in that we have added here the van den Bergh-Stothers values (van den Bergh 1977; Stothers 1983), lumped together in view of their exact agreement. Notice that the dV and vdB-S apparent distance moduli are indistinguishable, whereas the two scales differ by only 0.05 mag in foreground reddening. Given the widths of the evolved main sequences this color difference does not appear fundamental to the age determination.

Figures 4*b* and 5*b* show the CMD for NGC 419 and NGC

TABLE 2  
DISTANCE AND REDDENING SCALES

$(m-M)_0$	$(m-M)_{Av}$	$E(B-V)$	Sources
19.27.....	19.33	0.02	Sandage and Tammann 1974 (ST)
18.62.....	18.85	0.08	de Vaucouleurs 1978 (dV)
18.82.....	18.91	0.03	van den Bergh 1977, Stothers 1983 (vdB-S)

1984ApJ...283...552D

416, respectively, with the Yale isochrones (Ciardullo and Demarque 1977) superimposed for the two extreme scales of Table 2 (i.e., ST and dV). For consistency with Paper I we have retained the labeling of the absolute axes in the dV scale. As in Paper I, where we dealt with the younger field main sequence, we notice here that we cannot fit the evolved main sequence to the ST scales for any reasonable interval in composition.

i) NGC 419

The best fit to the Yale isochrones on the dV scale, using  $Z = 0.004$  (Fig. 4b) corresponding to  $[\text{Fe}/\text{H}] = -0.7$  (assuming  $Z_{\odot} = 0.02$ ), gives an age of 1.3 Gyr. From Figure 4d the best fit implies an age of 1.0 Gyr for a metallicity of  $Z = 0.01$  (i.e.,  $[\text{Fe}/\text{H}] = -0.3$ , which corresponds to half of the solar value). The fit for  $Z = 0.001$  ( $[\text{Fe}/\text{H}] = -1.3$ ) is of lower quality than the others, as expected from the results of § IVb. We adopt an age of  $1.2 \pm 0.5$  Gyr for NGC 419.

ii) NGC 416

A direct comparison of the diagrams indicates that NGC 416 is significantly older than NGC 419 in that its termination point is fainter and redder. Notice that although the shape of the bottom region of Figures 5b, 5c, 5d, reflects the normal accumulation of errors near the plate limit, the concentration of stars at  $V \sim 20.5$ ,  $B - V \sim 0.5$  is real, as discussed earlier. Taking the mean values of the best fits to Figures 5a and 5b, we estimate an age of  $2.5 \pm 0.7$  Gyr for NGC 416, the error reflecting the combined uncertainties.

#### V. SUMMARY AND DISCUSSION

The interpretation of the CMDs for NGC 419 and NGC 416 in terms of ages and abundances depends critically on the solution of two basic problems. First, the properties of the clusters must be isolated from those of the field. The study of the field itself is of great interest as a probe of the stellar formation process in the SMC and has been carried out in Paper I. Second, a number of scales must be established with some degree of certainty—metallicity, reddening, and distance—prior to the application of the standard model-fitting procedure.

Of all these problems the first one turned out to be the simplest. For NGC 419 the turnoff is now very well determined, and the identification of the cluster as an intermediate-age one belonging to Hodge's "billion year old" group (Hodge 1983) is well established. In the case of NGC 416, although the statistics near the termination point of the main sequence are less precise, the presence of a sequence which is fainter and redder than that of NGC 419 is secure and not an artifact of the field subtraction process. The age differential between the clusters amounts to roughly 1.5 Gyr, from the Yale isochrones, independently of the absolute distance scale. The existence of an age difference was to be expected on the basis of the number of known very red giants and carbon stars present in both clusters. Indeed, Blanco and McCarthy (1983) found no carbon stars in NGC 416 and at least six in NGC 419. From a study of red giants in the Magellanic Clouds, Aaronson and Mould (1982) found 18 stars in NGC 419 with  $B - V > 1.5$  and none in NGC 416. These differences are significant because NGC

419 is only 1 mag brighter in integrated  $B$  light than NGC 416 (Gordon and Kron 1983). Our data, on the other hand, are not appropriate to study the statistics of the extended giant branch because of the exclusion of stars which are very bright in  $V$  light, and therefore saturated, and the exclusion of the inner parts of the clusters. Our results are, in any case, qualitatively consistent with the conclusions by Aaronson and Mould (1982) that NGC 416 is older than NGC 419, although their value of 11 Gyr for the former is clearly excluded by our CMDs.

The fundamental problem in establishing absolute ages for the clusters remains that of the distance and reddening. We are puzzled by our result that the dV and vdB-S scales are more appropriate than the ST ones, as noticed in Paper I, because Hodge (1981) finds the opposite effect in fitting NGC 152 to the Yale isochrones. Comparing our diagrams to his Figure 5, we observe that the main sequence of NGC 419 is  $\sim 0.3$  mag redder than that of NGC 152, whereas the color of its core-helium-burning "clump" is about 0.2 mag bluer. Since the magnitude of the clump remains constant past the age of NGC 152 (Flower 1984), part of the discrepancy can be ascribed to age and metallicity effects on the main sequence, NGC 152 being younger than NGC 419. Other than that, and barring unexpected photometric errors in the zero point of our respective scales, a combination of differential reddening and *in-depth effects* may be present. One should keep in mind that NGC 152 is located on the side of the SMC opposite to where our clusters lie. The Wing area of the SMC studied here is distorted in shape and may belong to an intermediate-distance extension linking the two Magellanic Clouds.

The main conclusion of this investigation are: (1) NGC 416 is about 1.5 Gyr older than NGC 419; (2) the clusters' absolute ages are  $2.5 \pm 0.7$  Gyr and  $1.2 \pm 0.5$  Gyr, respectively, from a fit to the Yale isochrones, and area, therefore, younger than the old field population described in Paper I; (3) their metallicities are higher than  $[\text{Fe}/\text{H}] = -1.0$ , from integrated Washington photometry. We must add that our ages are too young by one step with respect to the calibration of the Searle, Wilkinson, and Bagnuolo (1980) classes versus ages, in the LMC, published by Cohen (1982), NGC 419 being class V and NGC 416, class VI in the SWB scheme. Since the mean metallicities of clusters in the SMC seem to be lower, for a given age, than in the LMC, we believe that the discrepancies could be explained as a combination of the intrinsic scatter of her Figure 2 with a metallicity offset. Because integrated photometry is feasible to very low apparent magnitudes, any calibration of integrated photometric indices versus age and/or metallicity, which can be performed in the Magellanic Clouds, is of fundamental importance in the study of more distant unresolved galaxies.

D. D. is grateful to the Federal and Provincial Governments for the tenure of Graduate Fellowships. E. H. wishes to thank the director of the Mount Wilson and Las Campanas Observatories for the granting of observing privileges at Las Campanas. E. H. also acknowledges the hospitality of ESO during the initial phase of this project.

This investigation was supported by the National Science and Engineering Research Council of Canada.

#### REFERENCES

- Aaronson, M., and Mould, J. 1982, *Ap. J. Suppl.*, **49**, 161.  
 Arp, H. 1958a, *A.J.*, **63**, 273.  
 ———. 1958b, *A.J.*, **63**, 487.  
 Blanco, V. M., and McCarthy, S. J. 1983, *A.J.*, **88**, 1442.

- Brück, M. T., and Hawkins, M. R. S. 1981, in *IAU Colloquium 68, Astrophysical Parameters for Globular Clusters*, ed. A. G. D. Philip and D. S. Hayes (Schenectady: L. Davis Press), p. 261.  
 Brück, M. T., and Marsoglu, A. 1978, *Astr. Ap.*, **68**, 193.

- Canterna, R. 1976, *A.J.*, **81**, 228.  
 Ciardullo, R. B., and Demarque, P. 1977, *Trans. Yale Obs.*, Vol. **33**.  
 Cohen, J. C. 1982, *Ap. J.*, **258**, 143.  
 de Vaucouleurs, G. 1978, *Ap. J.*, **223**, 730.  
 Durand, D. 1982, M.Sc. thesis, Université Laval.  
 Flower, P. J. 1984, *Ap. J.*, **278**, 582.  
 Gascoigne, S. C. B., Bessel, M. S., and Norris, J. 1981, in *IAU Colloquium 68, Astrophysical Parameters for Globular Clusters*, ed. A. G. D. Philip and D. S. Hayes (Schenectady: L. Davis Press), p. 223.  
 Gordon, K. C., and Kron, G. E. 1983, *Pub. A.S.P.*, **95**, 461.  
 Hardy, E. 1981, *A.J.*, **86**, 217.  
 Hardy, E., and Durand, D. 1984, *Ap. J.*, **279**, 567 (Paper I).  
 Hardy, E., Melnick, J., and Rhéault, C. 1980, in *IAU Symposium 85, Star Clusters*, ed. J. E. Hesser (Dordrecht: Reidel), p. 343.  
 Harris, H. C., and Canterna, R. 1977, *A.J.*, **82**, 798.  
 Hodge, P. W. 1981, *Ap. J.*, **247**, 894.  
 ———. 1983, *Ap. J.*, **264**, 470.  
 King, I. 1966, *A.J.*, **71**, 64.  
 Rhéault, C., and Hardy, E. 1980, in *Application of Digital Image Processing to Astronomy, Proc. Soc. Photo-Opt. Instrum. Eng.*, **264**, 200.  
 Sandage, A., and Tammann, G. A. 1974, *Ap. J.*, **190**, 525.  
 Searle, L., Wilkinson, A., and Bagnuolo, W. G. 1980, *Ap. J.*, **239**, 803 (SWB).  
 Stetson, P. B., and Harris, W. E. 1977, *A.J.*, **82**, 954.  
 Stothers, R. B. 1983, *Ap. J.*, **274**, 20.  
 van den Bergh, S. 1977, in *IAU Colloquium 37, Décalages vers le rouge et expansion de l'univers*, ed. C. Balkowski and B. E. Westerlund (Paris: Centre National de la Recherche Scientifique), p. 13.  
 Walker, M. F. 1972, *M.N.R.A.S.*, **159**, 379.

DANIEL DURAND: Département de physique, Faculté des sciences et de génie, Université Laval, Québec, P.Q. G1K 7P4, Canada

EDUARDO HARDY: Mount Wilson and Las Campanas Observatories, 813 Santa Barbara Street, Pasadena, CA 91101-1292

JORGE MELNICK: Observatorio Astronomico Nacional, Universidad de Chile, Casilla 36-D, Santiago, Chile